Growth and characterization of 3C–SiC and 2H–AlN/GaN films and devices produced on step-free 4H–SiC mesa substrates

P G Neudeck[1], H Du[2], M Skowronski[2], D J Spry and A J Trunek[3]

[1] NASA Glenn Research Center, 21000 Brookpark Road, MS 77-1, Cleveland, OH 44135, USA
[2] Department of Materials Science and Engineering, Carnegie Mellon University, Pittsburgh, PA 15213, USA
[3] OAI, NASA Glenn Research Center, 21000 Brookpark Road, MS 77-1, Cleveland, OH 44135, USA

E-mail: Neudeck@nasa.gov and mareks@cmu.edu

Abstract
While previously published experimental results have shown that the step-free (0 0 0 1) 4H–SiC mesa growth surface uniquely enables radical improvement of 3C–SiC and 2H–AlN/GaN heteroepitaxial film quality (>100-fold reduction in extended defect densities), important aspects of the step-free mesa heterofilm growth processes and resulting electronic device benefits remain to be more fully elucidated. This paper reviews and updates recent ongoing studies of 3C–SiC and 2H–AlN/GaN heteroepilayers grown on top of 4H–SiC mesas. For both 3C–SiC and AlN/GaN films nucleated on 4H–SiC mesas rendered completely free of atomic-scale surface steps, TEM studies reveal that relaxation of heterofilm strain arising from in-plane film/substrate lattice constant mismatch occurs in a remarkably benign manner that avoids formation of threading dislocations in the heteroepilayer. In particular, relaxation appears to occur via nucleation and inward lateral glide of near-interfacial dislocation half-loops from the mesa sidewalls. Preliminary studies of homojunction diodes implemented in 3C-SiC and AlN/GaN heterolayers demonstrate improved electrical performance compared with much more defective heterofilms grown on neighbouring stepped 4H–SiC mesas. Recombination-enhanced dislocation motion known to degrade forward-biased 4H–SiC bipolar diodes has been completely absent from our initial studies of 3C–SiC diodes, including diodes implemented on defective 3C–SiC heterolayers grown on stepped 4H–SiC mesas.

1. Introduction

The ability to grow high-quality heterocrystals would clearly enable important technological benefits, particularly in the semiconductor electronics industry. This realization has driven decades of materials research towards the attainment of improved semiconductor crystal heteroepilayers. Some important benefits of heteroepilayers to electronics and optoelectronics have been enabled even with limited quality and combinations of materials realized to date. The ability to heteroepitaxially join far broader ranges of materials, coupled with far fewer extended crystal defects, would undoubtedly unlock an abundance of even more beneficial technological capability.

Essentially all previous efforts to grow heteroepitaxial films, using a wide variety of crystalline materials over the past few decades, have initiated from substrate surfaces with abundant atomic scale steps. Some previous works, including [1, 2], have suggested that crystal growth surfaces completely free of atomic scale steps would beneficially reduce extended defect densities in subsequently deposited heteroepitaxial films. In particular, these past studies point out that a step-free growth surface should alleviate stacking mis-registration that occurs when two heterogrowth islands nucleated with a substrate growth step between them subsequently coalesce. Until recently however, there was no known means of actually producing such a 'step-free' crystal growth surface of sufficient area to support material studies and device fabrication.

Within the last few years, our research group at NASA Glenn pioneered the ability to produce patterned arrays of device sized (up to 0.4 mm ×0.4 mm) 4H–SiC and 6H–SiC mesas with silicon-face (0 0 0 1) top surfaces entirely free of atomic scale steps [3, 4]. The experimental details of this step-free mesa growth process have been extensively reported in [3, 5, 6]. These step-free mesa surfaces are produced on commercial on-axis 4H– or 6H–SiC wafers by first dry etching trench patterns into the wafer surface to form an array of thousands of isolated growth mesas on each wafer surface. The etch mask is wet-chemical stripped and the growth surface with pre-existing steps is prepared for growth using in-situ etching in the epitaxial growth reactor. Pure step-flow homoepitaxial growth is then carried out in low supersaturation growth conditions that effectively prevents two-dimensional (2D) island nucleation of new Si–C bilayers on terraces between existing growth steps. For mesas that are not threaded by substrate screw dislocations, the pure step-flow growth extends all pre-existing atomic scale surface steps on top of each mesa over to the mesa edge, leaving behind an array of mesas with top surfaces entirely free of atomic steps. Mesas in the array that happen to be threaded by one or more of the SiC wafer's randomly located screw dislocations cannot be rendered step-free, as these mesas evolve non-terminating growth spiral steps that routinely develop into hillocks (that are usually observable by differential interference contrast (DIC) optical microscopy).

Therefore, on any given 4H–SiC wafer sample subjected to our mesa-growth process, numerous 'control' 4H–SiC mesas that feature top surfaces with abundant atomic-scale growth steps (i.e. 'stepped mesas') can be found residing adjacent to numerous (0 0 0 1) 4H–SiC mesas with top surfaces completely free of atomic scale steps (i.e. 'step-free mesas'). When subjected to sufficient homoepilayer growth time (i.e. sufficiently beyond the growth time required for all pre-existing atomic scale steps to grow over to the mesa edge), step-free mesas exhibit readily observable differences in faceting and development of thin-lateral cantilevers compared with stepped mesas containing SiC substrate screw dislocations [7]. These differences remain observable even following growth of subsequent heteroepitaxial films on top of the mesas [5, 6, 8, 9], which in turn enables straightforward optical microscopy identification and characterization data/result sorting between stepped and step-free SiC mesas residing on the same SiC wafer.

The first experiments of growth and characterization of heteroepitaxial films on the newly available step-free 4H–SiC mesa surfaces have demonstrated amazingly successful improvements in heterofilm quality. Initial heteroepitaxial films of 3C–SiC as well as initial heterofilm layers of 2H–AlN (buffer layer)/2H–GaN grown on top of step-free 4H–SiC mesas have achieved more than 100-fold reductions in threading dislocation densities compared with heterofilm growth on surfaces with steps (including adjacent stepped 4H–SiC mesas on the same samples) [5, 6, 10–13]. The materials characterization of these initial mesa heterofilms that we have previously reported has been extensive. 3C–SiC mesa heterofilms were studied by atomic force microscopy (AFM), synchrotron white beam x-ray topography (SWBXT), high-resolution x-ray diffraction (HRXRD), cross-sectional transmission electron microscopy (XTEM), defect-preferential molten KOH-etching and thermal oxidation [5, 6, 8, 12–21], while the AlN/GaN mesa film quality has to date been studied via AFM and plan-view and cross-sectional TEM [8, 10, 11, 22]. The relevant references cited above contain additional information on each of the various characterization procedures employed in our studies. The results obtained by the various techniques have been cross correlated with each other and are fully consistent.

As an illustrative example of the dramatic benefits of using step-free mesas for heteroepilayer growth, figure 1 shows defect-preferential etching results (molten KOH [5, 13, 17]) recorded from adjacent 3C–SiC heterofilms nucleated on stepped (left) and step-free (right) 4H–SiC mesas subjected to otherwise identical processing. Ignoring the particulate contamination visible, the figure 1 right mesa surface contains only 7 (all triangular shaped) etch pit features. The left mesa of figure 1, whose 3C film was nucleated on a stepped 4H–SiC mesa (due to substrate screw dislocations), exhibits a much higher abundance of these triangular etch pits, in addition to straight and jagged trench features all arising from accelerated etching where various extended defects (to be described later in section 2.1) intersected the film surface. The extended defect density for the heterofilm grown on the stepped surface is clearly much greater (well over an order of magnitude difference) for the heterofilm nucleated on the stepped 4H mesa than for the film grown on the step-free 4H mesa. The result illustrated in figure 1 is representative of the behaviour that we have now observed repeatedly (on thousands of mesas spread across dozens of samples). These results indicate that the step-free mesa surface enables radically improved heteroepitaxy compared with conventional stepped growth surfaces.

Our collective experimental studies of 3C–SiC and AlN/GaN mesa film growth indicate that atomic-scale surface steps pose a large (perhaps dominant) impediment to ordered growth and relaxation of heteroepitaxial films. Despite the early achievements of these investigations, some physical limitations and mechanisms of step-free mesa growth processes remain to be more fully understood. This paper updates recent progress made in growth, characterization and understanding of high quality homoepitaxial and heteroepitaxial films grown on step-free 4H–SiC mesas.

2. Defect structure of 3C–SiC heterofilms on 4H–SiC

Some previous works have imprecisely stated that the in-plane lattice constants of all SiC polytypes are equal, implying that

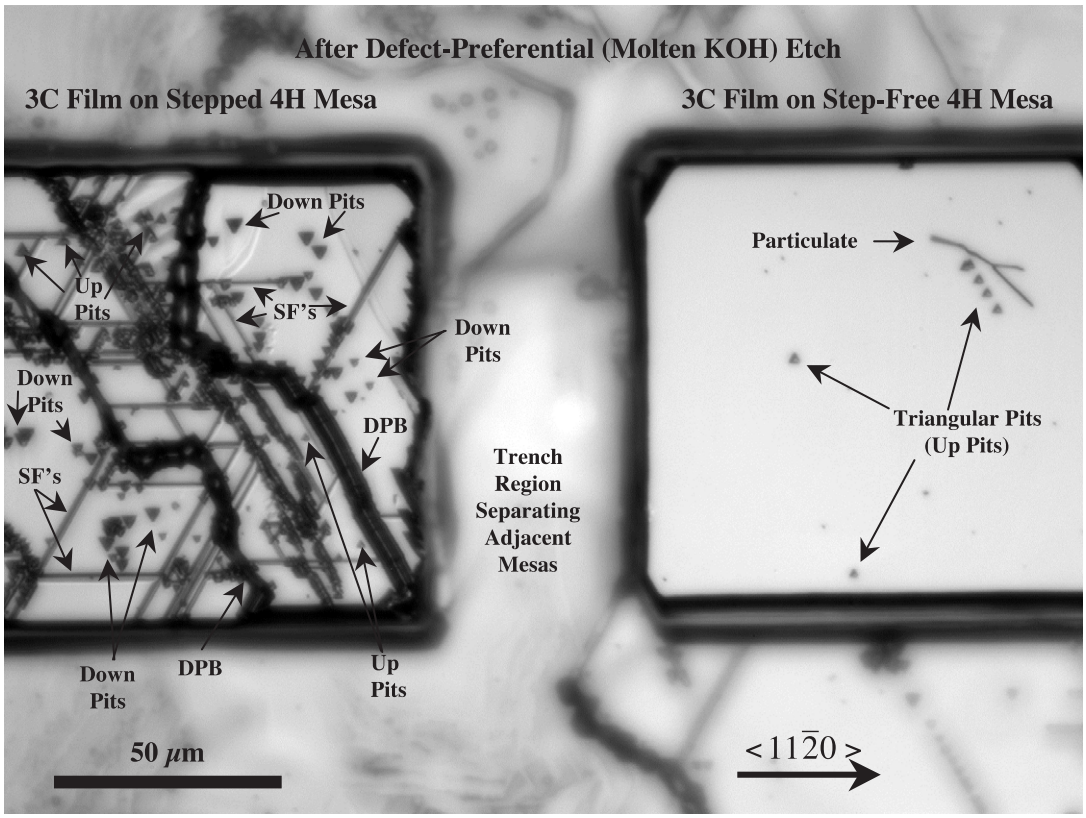

Figure 1. Optical micrograph of two adjacent 3C–SiC mesas heterofilms illustrating the drastic difference in extended defect structure revealed by defect-preferential etching. The highly defective 3C film on the left was nucleated on a 4H–SiC mesa with steps from a substrate screw dislocation, while the greatly improved 3C film on the right was nucleated on a 4H–SiC mesa completely free of atomic steps (see text).

strain buildup and relaxation effects would not be present when carrying out heteroepitaxy of different SiC polytypes. However, higher-accuracy HRXRD studies of SiC polytypes in the literature (such as [23–25]) measure experimentally significant differences between the in-plane lattice constants of different SiC polytypes. In this light, our collaborators at State University of New York (SUNY) at Stony Brook undertook detailed HRXRD studies of our 3C on 4H–SiC mesa heterofilms [18–20]. These studies conclusively showed experimentally important (0.01–0.08%) mismatch of in-plane lattice parameter between the 3C film and 4H mesa substrates, as measured on both stepped and step-free 4H–SiC mesas. Therefore, at least some relief of strain arising from in-plane lattice constant mismatch occurs in our 3C on 4H heteroepitaxial mesa growth. It therefore follows that dislocations arising from the heterofilm strain relief process can be expected in all of our mesa heterofilms (both 3C–SiC and III-N).

The following sections describe radical differences observed between the defect structure of heterofilms nucleated on step-free 4H–SiC compared with films nucleated on 4H-SiC mesas with steps. Possible mechanisms, some of which are related to radically different processes for strain relief between stepped and step-free heterointerfaces, are proposed within the framework of the experimental observations.

2.1. Defects in 3C–SiC heterofilms on stepped 4H–SiC mesas

The defect features commonly observed in 3C–SiC heterofilms grown on stepped 4H–SiC mesas (such as those illustrated in the figure 1 defect-preferential etch results) fall into three major categories corresponding to at least three types of extended crystal defects.

The small dark triangles seen on the etched 3C films of figure 1 are triangular etch pits (that are actually tetrahedral shape in three-dimensions, see figure 6 of [5] for SEM) that correspond to the intersection of a dislocation line with the film surface. Previously reported KOH etching of thin 3C–SiC films indicates that some of these triangular pits are threading edge dislocations inherited from the 4H–SiC substrate [5, 17]. However, the vastly higher density of pits observed for 3C films nucleated on stepped 4H mesas (figure 1, left) compared with 3C films on step-free 4H mesas (figure 1, right) indicates that the 4H substrate surface steps critically facilitate formation of abundant threading extended defects during the growth process in a manner that is effectively absent (or suppressed) for the step-free 4H nucleation surface. It is worth noting that only two orientations of triangular etch pits, designated 'up-pit' and 'down-pit' orientations in figure 1, are observed. These two etch pit orientations arise from the well-known fact that two variants of 3C stacking (one rotated 180° about the c-axis from the other) are possible for 3C polytpe nucleated on top of (0 0 0 1) hexagonal polytypes of SiC [26]. Therefore, the small triangular etch pits enable conclusive identification of the rotational 3C variant present across various regions of a highly defective 3C mesa heterofilm surface.

The highly jagged lines zigzagging through the left mesa of figure 1 are well known to be double-positioning boundary

(DPB) defects [5, 6, 27, 28]. As described in some previous works [5, 6, 21, 29], these defects are proposed to arise when multiple islands nucleate (and subsequently enlarge and coalesce) across atomic substrate terraces separated by steps with heights different from the substrate's c-axis unit-cell dimension. It is worth noting that additional DPB formation models have been proposed in which stacking errors occur during island nucleation on a (0 0 0 1) terrace [27, 30], with the implication that substrate step structure (e.g. step height) does not necessarily play a significant role. However, we contend that such an island nucleation stacking error mechanism cannot be the major DPB formation mechanism in our experiments, due to the lack of observed stacking errors and/or DPBs documented for our studies of island-nucleation-driven growth of 3C–SiC on step-free mesas. In other words, it is inconsistent for nucleation stacking errors to be causing the high densities of defects in 3C films grown on stepped 4H mesas (such as left mesa of figure 1), yet failing to induce the same defects in any observable quantity in 3C films grown (via the very same island-nucleation-driven process in identical growth conditions) on adjacent step-free 4H mesas (right mesa of figure 1).

The straight, well-oriented narrow trench features seen in the left mesa of figure 1 document enhanced etching at {1 1 1} stacking fault (SF) planar defects intersecting the 3C–SiC film surface [5, 13, 15]. As figure 1 illustrates (along with our previous works [5, 6, 12, 13]), these stacking faults are abundant for 3C films nucleated on stepped 4H–SiC mesas, and are very rare on properly nucleated 3C films on step-free 4H mesas. By the same line of reasoning argued above for DPBs, we contend that stacking errors in the island nucleation process (basic mechanism proposed by Booker and Sticker [31] for silicon) cannot be the cause for the vast majority of the stacking faults observed in our experiments, as such a mechanism would also be active (i.e. would create observable SFs) for the 3C film growths on step-free 4H mesas that are mostly (when properly nucleated) free of SFs. Therefore, we argue that the presence of 4H/3C heterointerface steps is a critical factor (either directly or indirectly) in SF formation. We have previously proposed one relatively simple model for 3C stacking fault formation during growth on a stepped 4H–SiC surface [5]. However, more rigorous atomic analysis and experimental documentation of such a model remain non-trivial challenges to be carried out in future works.

It is worth noting for the left mesa of figure 1 that all triangular etch-pits within any given continuous region in-between jagged DPB defects all have the same orientation (either all pointing 'up' or all pointing 'down' orientation within a region). Conversely, the triangular etch pits on opposite sides of jagged DPBs are oppositely oriented from each other, as they should be since the DPB is the border between regions of oppositely rotated 3C variants. The fact that no such change in triangular etch pit orientation is observed on opposite sides of any of the straight-line trenches in figure 1 serves as confirmation that these trenches arise due to SF defects instead of DPB defects in the 3C film.

Figure 2 shows XTEMs collected by our Carnegie Mellon University (CMU) co-authors from two defective 3C–SiC mesas nucleated on stepped 4H–SiC mesas. Faults along the {1 1 1} planes inclined (figure 2(a)) and parallel (figure 2(b)) to the 3C/4H heterointerface were observed. Some inclined faults terminate on other more prolonged faults, such as SF3 seen terminating on its intersection with SF1 in figure 2(a). Some of the inclined faults (such as SF1 and SF2 of figure 2(a)) propagate through the majority of the 3C–SiC film thickness, from very near the 3C/4H heterointeface up to the top surface of the 3C–SiC film. Such behaviour is perhaps somewhat expected given the apparent importance of the 3C/4H heterointerface step structure to 3C film quality. However, the presence of 3C/4H interfacial step S (shown at high resolution in figure 2(a) upper inset) does not directly correspond with the location of the lowermost extent of fault SF1 (that disappears from the sample above the 4H interface, shown at high resolution in figure 2(a) lower inset) in the cross-section. Such a non-correspondence between heterointerface step and film SF is perhaps expected given the extreme thinness of the XTEM specimen compared with the potential length dimensions (perpendicular to the thin cross-section) of both the heterointerfacial step edge and the propagating fault. In any event, further work is necessary to experimentally document the SF defect formation process.

2.2. Defect structure of 3C–SiC heterofilms on step-free 4H–SiC mesas

As we have previously reported [5, 6, 12, 13], the majority of properly nucleated 3C on step-free 4H mesa heterofilms are completely free of DPB and SF defects. Most of these 3C mesas exhibit a few (typically 1 to 10 for 100 μm^2 area) triangular etch pits. Initial KOH etching studies indicated that a majority of these arose from threading edge dislocations from the 4H–SiC substrate that propagated into the overlying 3C–SiC heterofilm [5, 17].

One limitation of defect-preferential etching techniques is that they do not necessarily reveal extended defects propagating in crystal planes parallel to, but well beneath, the heterofilm surface (for example, SFs shown in figure 2(b) for 3C film on stepped 4H mesa). This section summarizes cross-sectional TEM studies of 3C–SiC mesa heterofilms on step-free 4H–SiC mesas that would reveal the presence of such a defect structure.

Figure 3 shows XTEM characterization conducted by our CMU co-authors on a thick 3C–SiC film grown on a step-free 4H–SiC (75 μm $\times$ 205 μm pre-growth dimensions) mesa that exhibited no etch pits following KOH etching. Figure 3 shows the low-magnification cross-sectional composite image of the entire mesa width. Some of the 3C layer was removed during the thinning process using ion beam milling. The maximum thickness of the 3C layer on the left side of the figure is approximately 15 μm. Careful inspection of the entire cross-section revealed contrast associated with extended defects only at the interface between 4H and 3C material. The cross-sectional volume of the 3C heteroepilayers is defect free, as all the wavy features are sample thickness variation fringe contrast artifacts. The imaging conditions were selected in such a way as to produce a sharp contrast of stacking faults (as seen in figure 2). In particular, the CMU co-authors have examined this and two other mesas for the presence of stacking faults perpendicular to the growth direction and parallel to the basal plane of the substrate. None of these mesas exhibited any

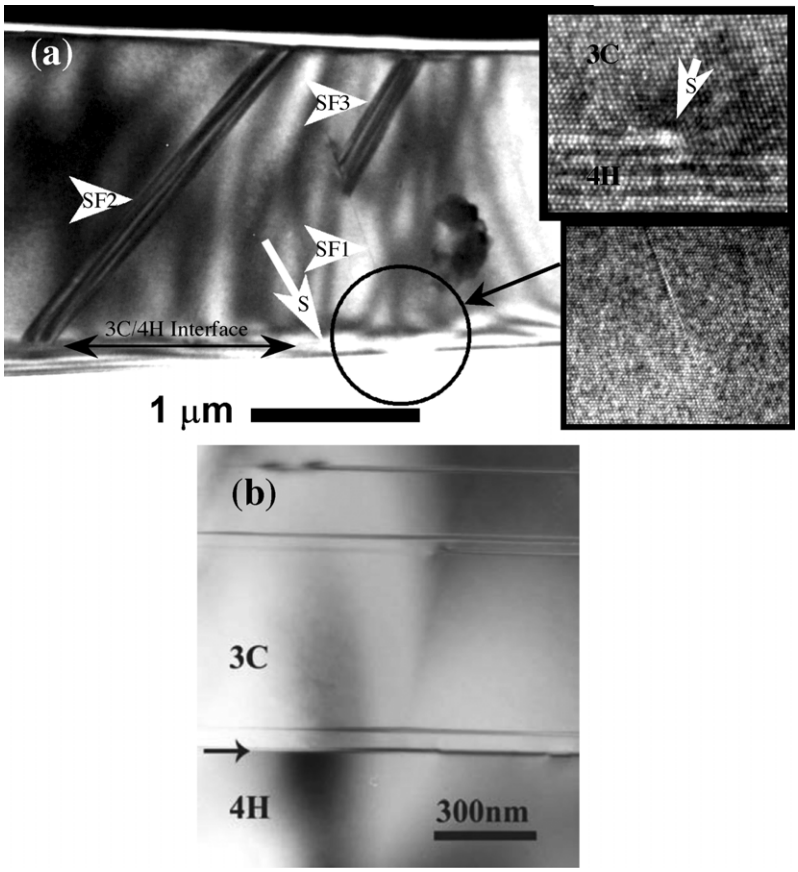

Figure 2. XTEMs of {1 1 1} stacking faults recorded by CMU in defective 3C–SiC films grown on stepped 4H–SiC mesas. (*a*) Inclined stacking faults, with stacking fault SF1 viewed edge-on. The upper inset shows a high resolution image of growth step S, while the lower inset shows a high resolution image of SF1 where it disappears in the circled region of 3C film above the 4H interface. (*b*) Stacking faults (viewed edge-on) propagating along the {1 1 1} plane parallel to the 3C/4H growth interface.

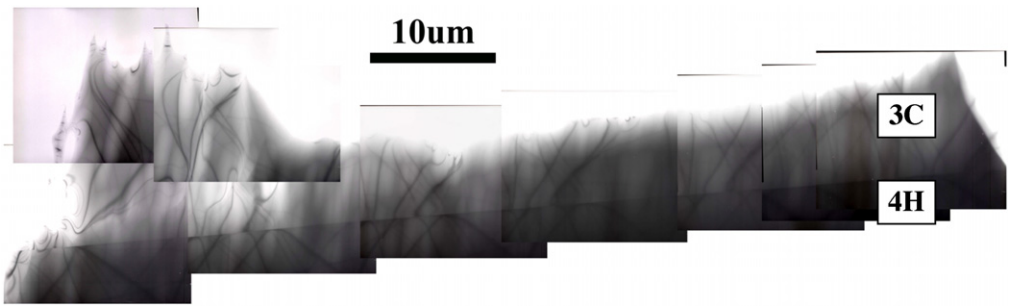

Figure 3. Composite XTEM image across thick 3C–SiC heterofilm grown on step-free 4H–SiC mesa. The 3C–SiC heteroepilayer is perfect cubic stacking throughout, completely free of SFs and other defects. The step-free 3C/4H heterointerface is clearly observed. Wavy features and non-uniform 3C film thickness are artefacts of specimen thinning process.

buried faults propagating parallel to the growth interface. It is evident that the stacking sequence throughout the entire 15 μm of the 3C growth corresponds to perfect 3C cubic polytype.

Figure 4 shows direct evidence of relaxation obtained through XTEM observation of misfit dislocations located at or close to the 3C/4H interface. The dislocation lines in figure 4(*a*) are either confined to the interface or very close to it with the line directions in all cases parallel to the interface. The dislocation lines are mostly parallel to each other. The separation distance (i.e. density) of the misfit dislocations falls within the range forecast by HRXRD studies (of other 3C/4H mesa samples) conducted by our SUNY collaborators [18–20]. It is interesting to note that the dislocations are located on the 4H side of the interface at a distance between 10 and 30 nm from the interface (figure 4(*a*)). Figures 4(*b*) and 4(*c*) present TEM images obtained in two beam conditions with the $\boldsymbol{g}$ vector either parallel or perpendicular to the interface (full analysis of the Burgers vector direction is impossible for this sample geometry). It is clear that the dislocation contrast with $\boldsymbol{g} = 1\bar{1}00$ is much stronger than for $\boldsymbol{g} = 0004$. This is a strong indication that the Burgers vector of this dislocation array is parallel to the

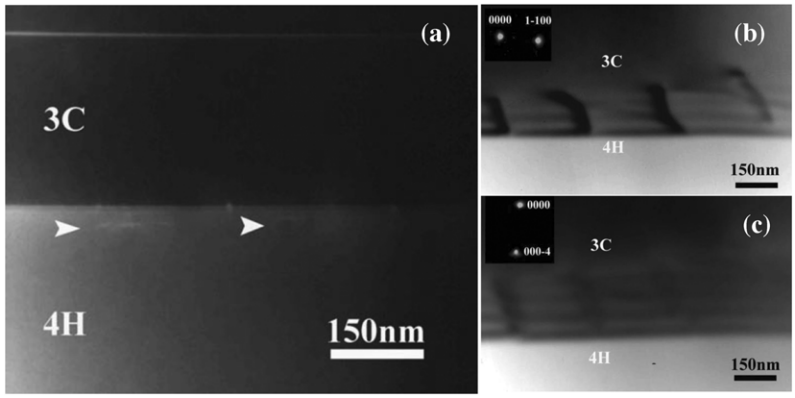

Figure 4. XTEMs of misfit dislocation array observed near 3C/4H heterointerface. (*a*) Bright field image viewed edge-on (near $\langle 1\,1\,\bar{2}\,0\rangle$ zone axis) showing dislocations reside on the 4H side of the 3C/4H heterointerface. Two beam dark field images (with sample slightly tilted to reveal dislocation lines) using reflections of (*b*) $(1\,\bar{1}\,0\,0)$ and (*c*) $(0\,0\,0\,4)$ strongly indicate that the dislocation Burgers vectors are parallel to the interface (see text). (*b*) and (*c*) reused with permission from [14], copyright 2006, Trans Tech Publications.

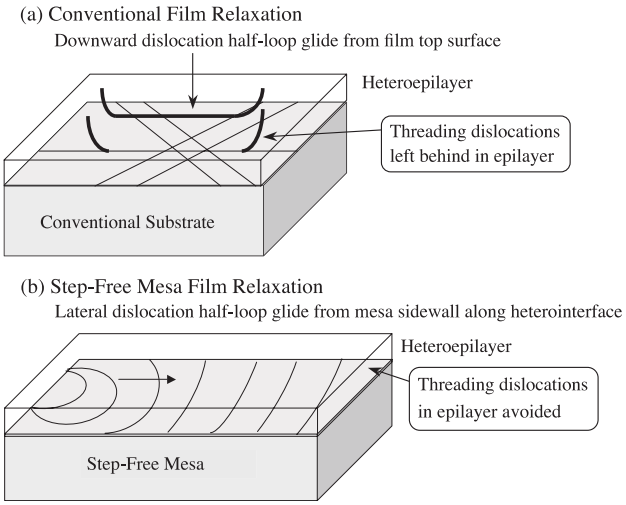

Figure 5. Schematic illustration comparing misfit strain relief mechanisms for heteroepitaxy carried out on (*a*) conventional substrates [32], and (*b*) step-free mesas [14].

interface. Although weaker, the contrast in figure 4(*c*) is not completely extinguished probably due to the mixed character of the dislocations.

2.3. Heterofilm relaxation model

The conventional model of stress relaxation in cubic semiconductor epilayers assumes that after the film thickness exceeds critical value, dislocation half loops nucleate at the film top surface and glide toward the interface along the inclined $\{1\,1\,1\}$ planes [32]. Consistent with the simplified depiction of figure 5(*a*), such a process is known to produce a high density of threading dislocation segments in the film and straight 60° misfit dislocations with Burgers vector inclined to the heterointerface. The above TEM observations of dislocations for the 3C on step-free 4H mesa case, including the absence of threading dislocations in 3C–SiC heterofilm and interfacial Burgers vectors parallel to the interface plane, are not consistent with this conventional model.

To explain the step-free mesa observations, our CMU colleagues instead proposed a new relaxation mechanism (figure 5(*b*)) in which dislocation half loops nucleate at mesa edges and then glide inward on planes parallel to the interface [14]. This mode of deformation is consistent with the primary slip system $\langle 1\,1\,\bar{2}\,0\rangle\{0\,0\,0\,1\}$ in 4H SiC or $\langle 1\,1\,0\rangle\{1\,1\,1\}$ in the 3C SiC. The resolved shear stress in the basal plane can be produced around the mesa edges by the misfit between polytypes. Relaxation by this mode does not leave threading dislocations in the film and the misfit dislocations may have mixed type with Burger's vectors in the basal plane. Therefore, the atomically flat interface appears to enable remarkably benign relaxation of 3C/4H lattice mismatch enabling greatly improved 3C-SiC heteroepitaxial quality.

3. Defect structure of AlN/GaN on 4H–SiC mesas

Because of larger mismatches in material properties, heteroepitaxial growth of III-N films on SiC is more challenging than growth of SiC heteropolytype junctions. Nevertheless, initial experiments in growing AlN/GaN films on stepped and step-free 4H–SiC mesas by our collaborators at the US Naval Research Laboratory (NRL) have yielded amazingly analogous behaviours as described above for 3C– on 4H–SiC mesa growth. First, as described by Bassim *et al* [10], initial growth experiments on step-free 4H–SiC mesas yielded a nearly 100-fold reduction in AlN/GaN threading dislocation density compared with growth on adjacent stepped 4H–SiC mesas. The TEM images in figure 6 (from [10, 22]) illustrate the large improvement in AlN/GaN film quality (∼100-fold reduction in film threading dislocation density) obtained by initiating growth on a clean step-free 4H–SiC mesa compared with a typical stepped 4H–SiC growth surface. In particular, screw-component dislocations were reduced to $\sim 1 \times 10^7\,\mathrm{cm}^{-2}$ for the step-free mesas compared with $\sim 2 \times 10^9\,\mathrm{cm}^{-2}$ obtained for comparable growth on stepped SiC surfaces [10]. Furthermore, plan-view TEM analysis of very thin AlN films revealed that remarkably ordered arrays of misfit dislocations formed near the SiC/AlN interface for growth on step-free 4H–SiC mesas [22]. Half loops were observed propagating inward from the edge of a mesa (figure 6(*f*)), which is quite consistent with the benign strain relaxation model depicted in figure 5(*b*). In contrast, TEM

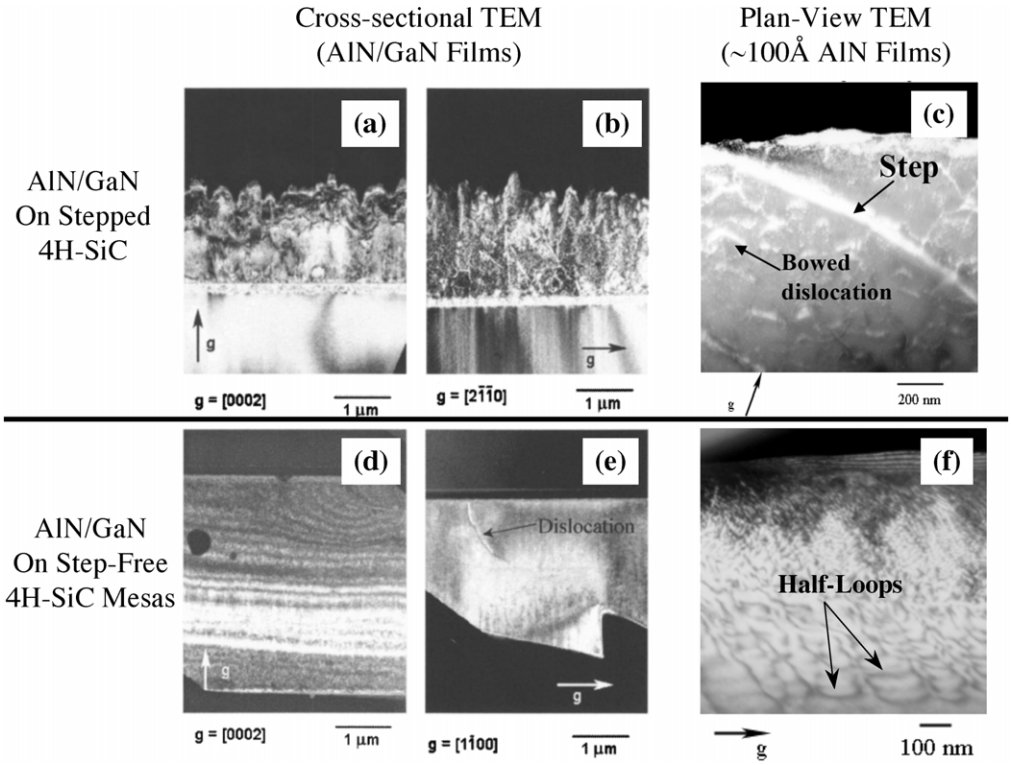

Figure 6. TEM results from growth and characterization of AlN/GaN films grown on (*a*)–(*c*) stepped and (*d*)–(*f*) step-free 4H–SiC mesa surfaces by NRL. The heterofilms grown on step-free 4H mesas exhibited ~100-fold reduction in threading dislocation density. (*a*), (*b*), (*d*) and (*e*) reused with permission from [10] copyright 2005 American Institute of Physics. (*c*) and (*f*) reused with permission from [22], copyright 2006, Trans Tech Publications.

images collected from low-coverage (~100Å) AlN grown on a nearby stepped 4H–SiC mesa (such as figure 6(*c*)) exhibited far more dislocations with far less order (including dislocation bowing). These results indicate that surface steps might pose a large (perhaps dominant) impediment to benign and ordered relaxation of heteroepitaxial films. On-going studies are attempting to gain further understanding of the misfit dislocation glide and its suspected interactions with heterointerfacial steps during epitaxial growth.

4. Initial electrical device results

A primary goal of realizing structurally superior heterocrystals is achieving improvements in semiconductor electronic device performance. This section summarizes the first preliminary electrical studies of improved 3C–SiC and AlN/GaN heterocrystals grown on 4H–SiC mesa substrates. All semiconductor diodes and transistors contain rectifying junctions (either unipolar or bipolar) that are critical to electrical device operation. Therefore, our initial device studies of the mesa heteroepilayers have focused on documenting the electrical characteristics of these fundamental rectifying Schottky and pn junctions. It is important to note that these studies are homojunction (instead of heterojunction) device studies, as the electrically dominant junction depletion regions are designed to reside entirely within the heteroepilayer without reaching the material heterojunction formed with the 4H substrate.

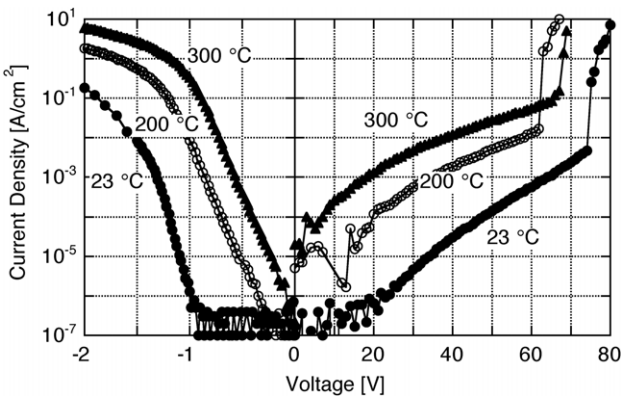

Figure 7. Log-scale IV characteristics of a 1.7×10^{17} cm^{-3} p-type (boron-doped, $A = 1 \times 10^{-4}$ cm^2) 3C–SiC Schottky diode grown on a step-free 4H–SiC mesa. After [33], copyright 2004, Trans Tech Publications.

4.1. Rectification properties of 3C–SiC diodes

Figure 7 summarizes the representative measured current versus voltage (IV) properties of boron-doped p-type 3C–SiC mesa Schottky diodes reported in [33]. Figure 8 summarizes the reverse IV properties of p$^+$n 3C–SiC diodes reported in [34]. The corresponding breakdown electric field of these devices resides well above the breakdown field of silicon but well below the breakdown field of 4H–SiC in the ⟨0 0 0 1⟩ direction. These rectification properties are superior (in combined terms of breakdown electric field and pre-

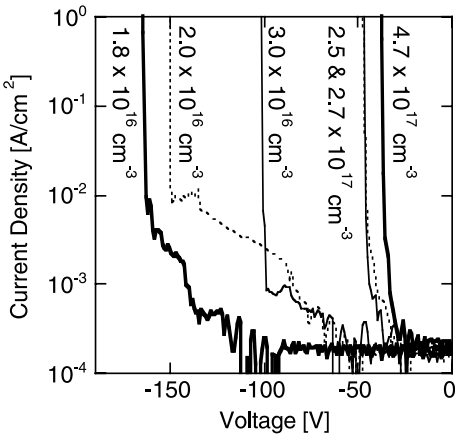

Figure 8. Log-scale reverse IV characteristics of 3C–SiC p$^+$n diodes (for a range of n-layer dopings shown on figure, $A = 5.6 \times 10^{-5}$ cm^2) grown on step-free 4H–SiC mesas. After [34], copyright 2006, Trans Tech Publications.

breakdown reverse leakage current density) to any previously reported [35, 36] for 3C–SiC, which reflects the superior crystal quality of the 3C–SiC grown on step-free 4H–SiC. In these initial experiments, there was no attempt to employ any form of junction edge termination in order to obtain an optimum reverse blocking voltage performance. Therefore, the blocking performances reported here represent a minimum demonstrated 'floor' for the material, which conceivably could be improved upon in future devices by employing properly optimized edge termination processing.

Despite the good blocking performance of these initial 3C–SiC diodes, imperfect diode IV behaviours nevertheless persist in the form of undesirably high (>2) forward ideality factors, undesirably high pre-breakdown reverse leakage current (especially at high temperature), and reduced breakdown voltage with increasing temperature (i.e. negative temperature coefficient of breakdown voltage). Far more comprehensive studies of many more devices are needed in order to determine the causes for these non-idealities. For example, device behaviour as a function of size, surface passivation and triangular etch pit content (which would require destructive KOH etching) would need to be investigated.

4.2. Forward-bias study of 3C–SiC diodes: lack of degradation and defect motion

In recent years, the commercialization of 4H–SiC bipolar power devices (diodes and transistors) has been prevented by the recombination enhanced dislocation glide (REDG) phenomenon that undesirably increases the forward voltage required for a device pn junction to conduct a given current in forward bias [37–40]. In particular, electron-hole recombination in forward-biased 4H–SiC pn junctions (at current densities as low as 0.1 A cm^{-2}) drives motion of partial dislocations resulting in localized transformations of hexagonal-stacked bilayers into cubic-stacked bilayers. This forms quantum wells that impede the transport of carriers through the device. In addition to monitoring the increase in forward voltage as a function of time, the dislocation motion/fault expansion can be tracked as it is happening in a forward-biased device via electroluminescence (EL) mapping [41, 42].

By starting with a SiC crystal structure that is entirely cubic, we previously speculated that the REDG degradation mechanism plaguing 4H–SiC bipolar devices might be absent from 3C–SiC bipolar device structures [6]. We have begun to test this hypothesis using EL and IV techniques nearly identical to those employed for observing REDG degradation in 4H–SiC diodes. Preliminary tests of 3C–SiC p$^+$n forward bias diode stability were conducted on one wafer using devices grown on both stepped and step-free 4H–SiC mesas [34, 43]. Figure 9 illustrates the basic results obtained for all 30 devices tested to date (all from the same wafer). Figure 9(*a*) shows a 'pre-stress' EL image of the device acquired at 10 A cm^{-2} at the very beginning of electrical testing. Figure 9(*b*) shows the EL image of the device 'post-stress' after it was subjected to a forward bias test regimen well in excess of stresses reported to degrade 4H–SiC pn diodes (10 min at 1 A cm^{-2}, 5 min at 10 A cm^{-2}, 5 min at 100 A cm^{-2}, and 2.5 min at 1000 A cm^{-2}). The bright features in the figure 9(*a*) and (*b*) EL images arise from in-grown defects (stacking faults) in this 3C film due to the fact that this mesa heterofilm was nucleated on a stepped 4H–SiC mesa. The pre-stress (figure 9(*a*)) and post-stress (figure 9(*b*)) EL images are identical, indicating that no motion or expansion of these defects occurred. Furthermore, as illustrated in figure 9(*c*), no appreciable change (i.e. increase) in forward voltage was observed for any of the stress current densities tested. For high-quality 3C diodes grown on step-free mesas, no bright line EL features were observed or spontaneously generated. Figure 9(*d*) shows the uniform yellow/green light emission recorded at 100 A cm^{-2} from a 3C–SiC diode grown on a step-free 4H–SiC mesa.

These preliminary 3C–SiC diode results stand in sharp contrast to stacking fault expansion and partial dislocation motion readily observed in 4H–SiC bipolar devices. However, further testing of many more devices from other wafers using higher-voltage and larger-area 3C–SiC bipolar devices remains to be carried out.

4.3. Improved AlN/GaN UV LED light emission efficiency

In a recent preliminary study [9], our collaborators at NRL compared the light emission characteristics of pn-junction ultraviolet light emitting diodes (UV LEDs) made from GaN heteroepilayers nucleated on stepped and step-free 4H–SiC mesas. Even though the fabrication was incomplete in that the metallurgical pn GaN junctions were not etch-isolated from uncontrolled edge deposition occurring at the periphery of the SiC growth mesas, significant improvement (49% on average) in UV light emission efficiency was nevertheless observed for the LEDs on step-free 4H mesas compared with neighbouring devices produced on nearby stepped 4H–SiC mesas. Figure 10(*a*) shows one comparison of nearby step-free and stepped 4H-mesa devices with similar forward IV characteristics [9]. At 100 A cm^{-2}, a 37% improvement in UV EL intensity is observed for this particular GaN device on the step-free 4H mesa compared with the nearby stepped-mesa control device. The ratio of desired UV EL to undesired (parasitic) yellow-band EL is also slightly improved for the step-free mesa device. As shown in the figure 10(*b*) histogram,

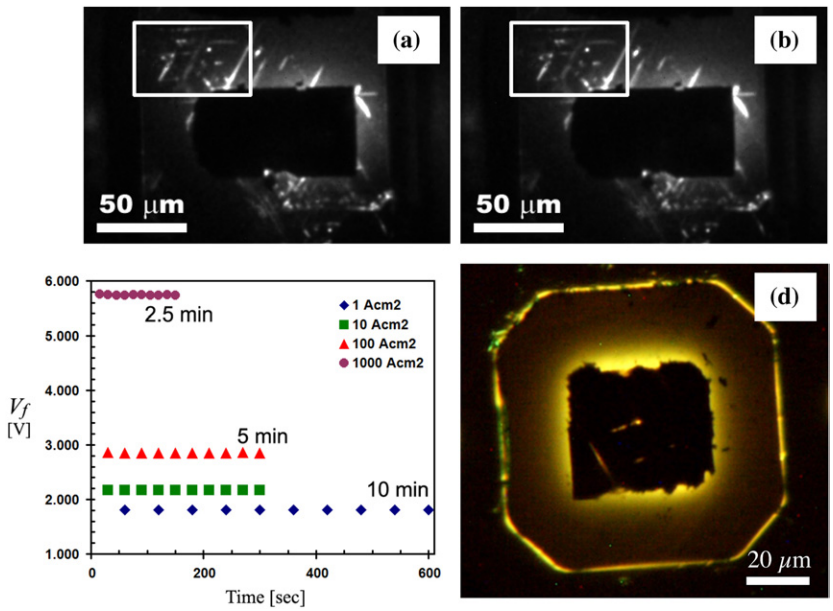

Figure 9. EL images (10 A cm^{-2}) of a defective 3C–SiC pn diode grown on stepped 4H–SiC mesa (*a*) at beginning and (*b*) at end of forward bias electrical stress test. Bright lines in (*a*) and (*b*) are enhanced EL at SF defects, but (in contrast to 4H pn diodes) there is no motion of these defects under forward bias stress. (*c*) Plot of forward voltage (V_f) needed to maintain a fixed current density as a function of forward bias time in the defective 3C–SiC pn diode. (*d*) Colour image of uniform yellow/green EL at 100 A cm^{-2} from high-quality 3C–SiC pn diode grown on a step-free 4H–SiC mesa. (*a*)–(*c*) after [43], copyright 2007, Trans Tech Publications. (Colour online.)

a consistent improvement of the UV EL was observed for comparable step-free versus stepped mesas at varying positions on the substrate, with an average improvement of 49% being observed at 100 A cm^{-2}.

The fact that the metallurgical GaN pn junction was not isolated from uncontrolled AlN and GaN deposition at the edges of the SiC growth mesas is believed responsible for at least some of the quantitative variability observed in this preliminary LED study. This hypothesis is supported by both optical beam induced current measurements that showed an order of magnitude increase in the photocurrent was observed in the edge regions, and the observed dependence of the reverse leakage current density on growth-mesa perimeter dimensions [9]. Further processing of these devices, in the form of an etch in order to mesa-isolate the GaN pn junctions from sidewall growth effects, has been initiated in order to better quantify the UV light emission properties of improved GaN realized on step-free 4H–SiC mesas.

5. Conclusion

Radical improvements to heteroepitaxial film quality, including over 100-fold reductions in heterofilm (both 3C–SiC and AlN/GaN) extended defect density, have been realized by carrying out heterofilm growth on top of 4H–SiC mesas whose top surfaces are completely free of atomic-scale steps. Material studies reviewed in this paper indicate that a remarkably different (not previously observed to our knowledge) and benign strain-relief takes place for mesa heterofilms nucleated on step-free 4H–SiC mesas compared with heterofilms nucleated on 4H–SiC mesas with atomic scale steps. For the step-free heterointerface, relatively ordered near-interfacial misfit dislocations appear to glide inward from the mesa sidewalls to relieve in-plane strain without leaving behind threading dislocations in the overlying heterofilm. Heterofilms nucleated on 4H–SiC mesas with steps exhibited a more conventional defect structure with abundant threading dislocations that were presumably left behind by conventional relaxation mechanisms involving downward dislocation glide from the heterofilm top surface.

Therefore, the use of the step-free 4H–SiC mesa growth surface uniquely enables well-ordered growth and strain relaxation to occur in a manner not possible or observed for conventional growth surfaces that have all had abundant atomic-scale substrate steps. In other words, dominant film strain relaxation ‘rules’ (i.e. physical mechanisms) previously accepted to have limited the structural quality of all previous heteroepitaxial films (exceeding critical thickness) appear to have been effectively circumvented (mostly) by the use of the step-free 4H–SiC mesa top as the growth template. At the very least, such rule-changing results present an exciting opportunity for development and beneficial realization of improved wide bandgap semiconductor heterocrystals and associated electronic devices (such as short-wavelength LEDs and lasers) whose performances are hindered by heterofilm crystal defects. Furthermore, we speculate that perhaps it might be possible to apply the step-fee mesa heteroepitaxial growth process to other material systems (such as silicon, diamond, ZnO, GaAs, etc.) [44]. The ability to heteroepitaxially join far broader ranges of materials, coupled with far fewer extended crystal defects, could perhaps unlock additional worthwhile technological benefits.

This paper has also described some promising preliminary mesa heterocrystal electrical device results. 3C–SiC diodes grown on step-free 4H–SiC mesas have exhibited improved current-voltage characteristics compared with all previously published 3C–SiC results. Furthermore, 3C–SiC pn junction diodes that were tested at current densities as high as

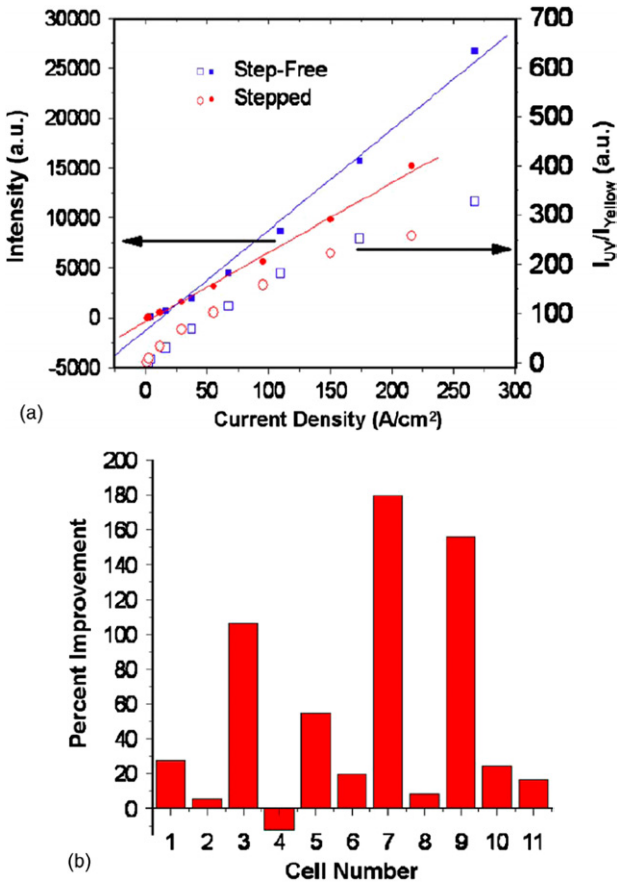

Figure 10. (*a*) Dependence of UV EL intensity (closed symbols, left axis) and the ratio of the UV to yellow EL Intensity (open symbols, right axis) as a function of current density for a step-free (blue squares) and a nearby stepped (red circles) mesa. (*b*) Histogram of the percent improvement of the UV EL output of a variety of step-free mesas in comparison with their stepped counterparts within various dies scattered across the wafer surface. Reused with permission from [9], copyright 2006, American Institute of Physics. (Colour online.)

1000 A cm^{-2} did not exhibit degradation of forward voltage that has plagued (and prevented commercialization of) 4H–SiC pn junction diodes. Finally, GaN pn junctions (incompletely isolated) with reduced threading dislocation density grown on step-free 4H–SiC mesas exhibited significantly improved UV electroluminescence compared with devices grown on stepped mesas.

Despite these initial accomplishments, the vast majority of work necessary to optimize and characterize step-free surface heteroepitaxial growth and devices remains to be carried out.

Acknowledgments

The authors would like to again acknowledge the fruitful collaborations referenced in this review paper from the wide bandgap research groups at the US Naval Research Laboratory, State University of New York at Stony Brook, and Case Western Reserve University. The work at NASA Glenn Research Center was carried out under the Ultra Efficient Engine Technology, Advanced Electrical Components, Revolutionary Aeropropulsion Concepts, and Director's Discretionary Funds projects. The authors wish to gratefully acknowledge the valuable assistance of J Anthony Powell, Michelle Mrdenovich, Beth Osborn, Emye Benavage, Drago Androjna, Glenn Beheim, Gary Hunter, Lawrence Matus, Kevin Speer, Brent Gardner, David Larkin, Kimala Laster, Charles Blaha, Mike Artale, Jose Gonzalez and Pete Lampard at NASA Glenn Research Center.

References

[1] Tanaka S, Kern R S and Davis R F 1995 *Appl. Phys. Lett.* **66** 37
[2] Yamada S, Kato J-i, Tanaka S, Suemune I, Avramescu A, Aoyagi Y, Teraguchi N and Suzuki A 2001 *Appl. Phys. Lett.* **78** 3612
[3] Powell J, Neudeck P, Trunek A, Beheim G, Matus L, R. Hoffman J and Keys L 2000 *Appl. Phys. Lett.* **77** 1449
[4] Powell J A, Larkin D J, Neudeck P G and Matus L G 1999 *US Patent* 5,915,194
[5] Neudeck P G, Trunek A J, Spry D J, Powell J A, Du H, Skowronski M, Huang X R and Dudley M 2006 *Chem. Vapor Depos.* **12** 531
[6] Neudeck P G and Powell J A 2003 *Recent Major Advances in SiC* ed W J Choyke *et al* (Heidelberg: Springer) p 179
[7] Neudeck P G, Powell J A, Beheim G M, Benavage E L, Abel P B, Trunek A J, Spry D J, Dudley M and Vetter W M 2002 *J. Appl. Phys.* **92** 2391
[8] Neudeck P G *et al* 2006 *Silicon Carbide 2006—Materials, Processing and Devices* (*Materials Research Society Symposium Proceedings* vol 911) ed T Kimoto *et al* (Warrendale, PA: Materials Research Society) p 85
[9] Caldwell J D *et al* 2006 *Appl. Phys. Lett.* **88** 263509
[10] Bassim N D, Twigg M E, Eddy C R Jr, Culbertson J C, Mastro M A, Henry R L, Holm R T, Neudeck P G, Trunek A J and Powell J A 2005 *Appl. Phys. Lett.* **86** 021902
[11] Eddy C R Jr, Bassim N D, Mastro M A, Henry R L, Twigg M E, Holm R T, Neudeck P G, Powell J A and Trunek A J 2006 *Silicon Carbide and Related Materials 2005* (*Materials Science Forum* vol 527–529) ed R P Devaty *et al* (Switzerland: Trans Tech Publications) p 1483
[12] Neudeck P G, Powell J A, Trunek A J, Huang X R and Dudley M 2002 *Silicon Carbide and Related Materials 2001* (*Materials Science Forum* vol 389-393) ed S Yoshida *et al* (Switzerland: Trans Tech Publications) p 311
[13] Neudeck P G, Powell J A, Spry D J, Trunek A J, Huang X, Vetter W M, Dudley M, Skowronski M and Liu J 2003 *Silicon Carbide and Related Materials—2002* (*Materials Science Forum* vol 433–436) ed P Bergman and E Janzen (Switzerland: Trans Tech Publications) p 213
[14] Du H, Skowronski M, Neudeck P G, Trunek A J, Spry D J and Powell J A 2006 *Silicon Carbide and Related Materials 2005* (*Materials Science Forum* vol 527–529) ed R P Devaty *et al* (Switzerland: Trans Tech Publications) p 279
[15] Trunek A J, Neudeck P G, Powell J A and Spry D J 2004 *Silicon Carbide and Related Materials 2003* (*Materials Science Forum* vol 457-460) ed R Madar*et al* (Switzerland: Trans Tech Publications) p 261
[16] Neudeck P G, Trunek A J and Powell J A 2004 *Silicon Carbide 2004—Materials, Processing and Devices* (*Materials Research Society Symposium Proceedings* vol 815) ed M Dudley *et al* (Warrendale, PA: Materials Research Society) p 59
[17] Neudeck P G, Powell J A, Trunek A J and Spry D J 2004 *Silicon Carbide and Related Materials 2003* (*Materials Science Forum* vol 457-460) ed R Madar *et al* (Switzerland: Trans Tech Publications) p 169
[18] Huang X R, Dudley M, Cho W, Okojie R S and Neudeck P G 2004 *Silicon Carbide and Related Materials 2003* (*Materials Science Forum* vol 457–460) ed R Madar *et al* (Switzerland: Trans Tech) p 157

[19] Huang X, Dudley M, Neudeck P G and Powell J A 2003 *Silicon Carbide 2002—Materials, Processing and Devices* vol 742, ed S E Saddow *et al* (Warrendale, PA: Materials Research Society) p K3.8.1
[20] Dudley M, Huang X, Vetter W M and Neudeck P G 2003 *Silicon Carbide and Related Materials—2002* (*Materials Science Forum* vol 433–436) ed P Bergman and E Janzen (Switzerland: Trans Tech Publications) p 247
[21] Dudley M, Vetter W M and Neudeck P G 2002 *J. Cryst. Growth* **240** 22
[22] Bassim N D, Twigg M E, Mastro M A, Neudeck P, Eddy C R Jr, Henry R L, Holm R N, Powell J A and Trunek A J 2006 *Silicon Carbide and Related Materials 2005* (*Materials Science Forum* vol 527–529) ed R P Devaty *et al* (Switzerland: Trans Tech Publications) p 1509
[23] Tairov Y M and Tsvetkov V F 1983 *Crystal Growth and Characterization of Polytype Structures* ed P Krishna (Oxford: Pergamon) p 111
[24] Gomes de Mesquita A H 1967 *Acta Cryst.* **23** 610
[25] Chien F R, Nutt S R and Yoo W S 1995 *J. Appl. Phys.* **77** 3138
[26] Powell J A, Pirouz P and Choyke W J 1993 *Semiconductor Interfaces, Microstructures, and Devices: Properties and Applications* ed Z C Feng (Bristol, UK: Institute of Physics Publishing) p 257
[27] Kimoto T, Itoh A and Matsunami H 1997 *Phys. Status Solidi* b **202** 247
[28] Powell J A, Petit J B, Edgar J H, Jenkins I G, Matus L G, Choyke W J, Clemen L, Yoganathan M, Yang J W and Pirouz P 1991 *Appl. Phys. Lett.* **59** 183
[29] Tyc S 1994 *Silicon Carbide and Related Materials: Proceedings of the Fifth International Conference* (*Institute of Physics Conference Series* no 137) ed M Spencer *et al* (Bristol, UK: Institute of Physics Publishing) p 333
[30] Speer K M, Neudeck P G, Crimp M A, Burda C and Pirouz P 2007 Possible formation mechanisms for defects observed in heteroepitaxially grown 3C–SiC *Phys. Status Solidi* c at press
[31] Booker G R and Stickler R 1962 *J. Appl. Phys.* **33** 3281
[32] Matthews J W and Blakeslee A E 1974 *J. Cryst. Growth* **27** 118
[33] Spry D J, Trunek A J and Neudeck P G 2004 *Silicon Carbide and Related Materials 2003* (*Materials Science Forum* vol 457–460) ed R Madar *et al* (Switzerland: Trans Tech) p 1061
[34] Neudeck P G, Spry D J and Trunek A J 2006 *Silicon Carbide and Related Materials 2005* (*Materials Science Forum* vol 527-529) ed R P Devaty *et al* (Switzerland: Trans Tech Publications) p 1335
[35] Neudeck P G, Larkin D J, Starr J E, Powell J A, Salupo C S and Matus L G 1994 *IEEE Trans. Electron Devices* **41** 826
[36] Nagasawa H, Yagi K, Kawahara T, Hatta N and Abe M 2006 *Microelectron. Eng.* **83** 185
[37] Ha S and J.P. B 2005 *MRS Bull.***30** 305
[38] Lendenmann H, Bergman J P, Dahlquist F and Hallin C 2003 *Silicon Carbide and Related Materials—2002* (*Materials Science Forum* vol 433-436) ed P Bergman and E Janzen (Switzerland: Trans Tech Publications) p 901
[39] Lendenmann H, Dahlquist F, Johansson N, Bergman J, Bleichner H and Ovren C 2000 *1st Int. Workshop on Ultra-Low-Loss Power Device Technology (Nara, Japan)* p 125
[40] Skowronski M and Ha S 2006 *J. Appl. Phys.* **99** 011101
[41] Galeckas A, Linnros J, Breitholtz B and Bleichner H 2001 *J. Appl. Phys.* **90** 980
[42] Stahlbush R E, Fatemi M, Fedison J B, Arthur S D, Rowland L B and Wang S 2002 *J. Electron. Mater.***31** 370
[43] Speer K M, Spry D J, Trunek A J, Neudeck P G, Crimp M, Hile J, Burda C and Pirouz P 2007 Absence of dislocation motion in 3C–SiC pn diodes under forward bias *Silicon Carbide and Related Materials 2006* (*Materials Science Forum)* ed N Wright *et al* (Switzerland: Trans Tech Publications) at press
[44] Powell J A, Larkin D J, Neudeck P G and Matus L G 2000 *USA Patent* 6,165,874